

Metal Oxide Nanotubes and Photo-Excitation Effects: New Approaches for Low-to-Intermediate Temperature Solid Oxide Fuel Cells

Investigators

Paul C. McIntyre, Associate Professor, Materials Science & Engineering; Michael Shandalov, Postdoc, Materials Science & Engineering; Nana Ayensu, Cynthia Ginestra, Irene Goldthorpe and Andy Lin, Graduate Researchers, Stanford University.

Abstract

During the first full year of this project, we made significant advances in 1) microfabrication of nanoscale planar metal oxide membranes, a key step in making micro solid oxide fuel cell (SOFC) test structures; 2) synthesis and microstructural characterization of metal oxide nanotubes; 3) development of new atomic layer deposition (ALD) processes for synthesis of yttria-stabilized zirconia SOFC membranes with improved membrane thickness and composition control; and 4) ALD of La and Sr oxides for growth of mixed ionic and electronic conducting $\text{La}(\text{Sr},\text{Co})\text{O}_3$ SOFC electrodes. Highlights included the demonstration of promising etch selectivity to metal oxide layers during microfabrication of planar SOFC electrolyte membranes on Si (100) wafers and successful wet-etching of Ge nanowire “cores” to produce HfO_2 metal oxide nanotubes from conformal ALD- HfO_2 shells grown around these wire templates. The latter work demonstrates a novel approach for producing high surface area electrolyte membranes, a potential route to SOFCs with increased power density. Research is now underway to combine the new ALD processes under development with these microfabrication and nanofabrication methods, produce both electrolyte and electrode structures with optimized properties. In parallel, we have been building up the capability to do routine through-thickness current-voltage characterization and impedance spectroscopy on microfabricated fuel cells in our laboratory. These capabilities will compliment the more sophisticated electrochemical measurements being done in the laboratory of our collaborator, Prof. Shriram Ramanathan, of Harvard University.

Introduction

The goal of this project is to enhance the power density and low-temperature efficiency of solid oxide fuel cells manufactured by atomic layer deposition. These enhancements will be achieved by engineering the morphology of the electrolyte at the nanoscale, and by studying the effects of photo-excitation on the catalytic properties of the membrane surface and on the concentration of electronic carriers and ionic defects in the thin film SOFC structure.

The efficiency of a fuel cell is limited by the loss mechanisms inherent to its operation. The power density of a fuel cell is limited by the area of its electrolyte membrane. These two operational parameters are related by the fact that thinner electrolytes not only limit the resistive losses within the fuel cell, but they also allow the incorporation of more active area into a given stack volume.

Ultra-thin electrolyte membranes for solid oxide fuel cells must meet at least two criteria: they must be free of pinholes through which gases could leak, and they must be

of the correct chemical composition and crystalline structure. Atomic layer deposition (ALD) is capable of making a pinhole-free layer of material 2 to 3 orders of magnitude thinner than state-of-the-art electrolyte membranes. Furthermore, this layer is highly conformal to the substrate, even over rough or convoluted surfaces. The chemical composition of the membrane is determined by the mix of precursors admitted to the deposition chamber, and it has been shown that the crystalline structure can be controlled through a sequence of deposition steps at different compositions and thicknesses, followed by annealing at a specified temperature.

Electrolyte thickness is not the only parameter that governs efficiency. The nature of the chemical reactions that take place at the surface of the membrane (the "triple phase boundary") is also responsible for lost work in a fuel cell. Absorption by surface chemical species of photons in the ultraviolet range may reduce the activation energy for these reactions or provide alternative reaction pathways, thereby improving cell efficiency. Illumination studies are also of fundamental interest as a means of altering the electronic carrier concentrations in metal oxides and thus, perhaps, the concentration of charged point defects.

Our research into novel structures for low-temperature SOFCs involves a thorough investigation of the properties of ALD fabricated yttria stabilized zirconia (YSZ) and related metal oxide membranes, and the associated microstructure-property relations. Working with our collaborators at Harvard, the oxygen ion-conductivity of the ultra-thin films will be compared to that reported for bulk crystals and ceramics.

A porous electrode layer must be applied to the surface of the electrolyte membrane for the fuel cell to be operational. The team will investigate the use of ALD to form a perovskite mixed electron-ion conductor layer for this purpose. Once a perovskite deposition process has been developed, the team will conduct experiments to determine both the oxygen diffusivity through the YSZ and the surface oxygen exchange kinetics on bare YSZ and on perovskite-coated YSZ.

While an increase in membrane performance can be achieved via reduction of its thickness, the major increase in membrane area proposed by this research will be achieved by forming the electrolyte as a series of YSZ nanotubes instead of planar YSZ sheets. The nanotubes will be manufactured by growing a forest of germanium nanowires on a silica substrate (Figure 1). This forest will act as a template, and the YSZ layer will be grown atop the germanium. The initial germanium nanowire outer diameter will thus define the inner diameter of the final metal oxide nanotubes. ALD-coated nanowires will then be released from the substrate surface by selective etching of the underlying silica and Ge nanowires.

Background

We are unaware of any publication on ALD-grown metal oxide nanotubes for use in SOFC applications, which is a main topic of research in this project, including important results this year. However, during the past year, in addition to our own publication,¹ two other groups have reported on the properties of planar ALD-grown YSZ electrolytes for

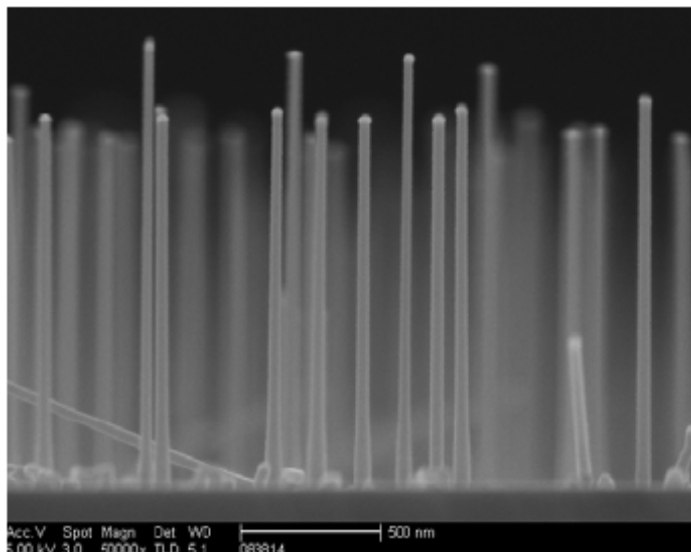


Figure 1: Dense array of Ge single crystal nanowires grown on a Si substrate. These wires are used as templates for atomic layer deposition of conformal metal oxide nanotubes, and are subsequently removed by selective wet-etching in $\text{H}_2\text{O}_2(\text{aq})$.

solid oxide fuel cell applications. The group of Cassir et al.² deposited relatively thick (300-1000 nm) $\text{Y}_2\text{O}_3/\text{ZrO}_2$ ALD laminates which they claimed were in the cubic structure (the oxygen fast ion conducting phase in bulk specimens), as-deposited at 300°C . However, the supporting x-ray diffraction data for the films' crystal structure were inconclusive. These authors also reported a 10 mol% Y_2O_3 composition for their laminate-derived films, but the energy dispersive spectroscopy analysis of the $\text{Y}_2\text{O}_3:\text{ZrO}_2$ ratio is actually rather uncertain because of Y and Zr peak overlap. Through-thickness impedance spectroscopy at temperatures in the range $100\text{-}350^\circ\text{C}$ suggested that the thinner films analyzed had higher electrical conductivities than the thicker ones and somewhat higher conductivities than bulk YSZ samples at this temperature. However, all films measured had a similar and surprisingly small (~ 0.35 eV) activation enthalpy for their conductivity. Bulk YSZ exhibits an activation enthalpy of ~ 1 eV. The much lower enthalpy detected in these experiments may indicate that at least a portion of the conduction measured by Cassir et al. is electronic rather than ionic.

The group Prinz and coworkers also published a paper³ outlining results obtained for ALD-grown YSZ films, in this case for thicknesses of 60 nm. Similar to the case of Cassir et al., this group also reported crystalline cubic YSZ alloys as-deposited. However, the x-ray diffraction peaks exhibited by their films were very weak and could possibly be indexed to other phases, such as tetragonal ZrO_2 . Using Si microfabrication methods similar to those we are pursuing in our own research, Prinz et al. prepared free-standing YSZ electrolytes sandwiched between porous Pt electrodes. They tested the films' current-voltage (I-V) behavior perpendicular to the plane of the free-standing film at temperatures in the range $250\text{-}400^\circ\text{C}$. Very promising fuel cell performance was reported, with maximum power densities near 300 mW/cm². Interestingly, the ALD films exhibited much higher power densities than comparable thickness YSZ electrolytes

deposited by the alternate method of sputter deposition. The large power densities did not appear to result from an unusually high ion conductivity, which was found by impedance spectroscopy to be comparable to that of bulk cubic YSZ at similar temperatures. Instead, for reasons were not elucidated, the ALD films exhibited extraordinarily high exchange current densities at the electrode/electrolyte interface.

In contrast to these results, our own work¹ indicates that the as-deposited laminate films are typically amorphous or, at best, weakly crystalline (the ZrO₂ component crystallizes preferentially at typical ALD deposition temperatures < 350°C). Transmission electron microscopy (TEM), electron diffraction, and secondary ion mass spectrometry indicated that high temperature anneals were required to crystallize and interdiffuse the Y₂O₃/ZrO₂ nanolaminates to produce homogeneous YSZ alloy electrolytes. Consistent with the low (2-3 mol%) Y₂O₃ composition of these films, they were in the tetragonal phase after the anneal. In-plane impedance spectroscopy conducted on these YSZ electrolytes indicated a larger ionic conductivity than expected for *tet*-YSZ of this composition at temperatures of 700-900°C. However, the activation enthalpy of the conductivity was higher than expected from bulk data (~ 2 eV rather than ~ 1 eV),⁴ suggesting that nanocrystalline size effects may alter the ionic conduction mechanism. Further work is needed to confirm the generality of these effects, by systematically studying the composition dependence of ionic conduction in ALD-YSZ.

Results

1. Microfabrication of ALD-Metal Oxide SOFC structures

Particularly thin (200 μm) double-side polished Si(100) wafers covered with Si₃N₄ 200 nm-thick layers deposited from both sides were used as mechanical support for free-standing HfO₂ ultra-thin membranes. Hafnia films were used because of the ease of deposition of these fluorite-structure films and their chemical similarity to YSZ, which will ultimately be used in our microfabricated SOFC's. In order to fabricate these ultra-thin SOFC membranes, the following process-flow was used (Fig.2).

Ultra-thin HfO₂ films with thicknesses ranging from 15 to 32 nm were grown by ALD using TDEAH and, recently, TDMAH volatile precursors on Si(100) wafers covered with Si₃N₄. As-deposited HfO₂ films had amorphous structure. The films were annealed at various temperatures ranging from 550 to 850°C in He atmosphere for 3 hrs. ALD-grown HfO₂ films showed very high degree of conformity with low roughness (will be shown in TEM results in section 2). HfO₂ films having thickness of 15-26 nm and annealed at 800 and 850°C for 3 hrs were fully crystalline (TEM results in section 2).

Square-shaped window pattern with various window sizes on Si₃N₄ back-side layer of the wafer was fabricated using standard optical lithography procedure following dry reactive ion etching (RIE) of Si₃N₄ layer. Standard nitride etch recipe was used by applying mixed CF₆ and O₂ plasma. Then, wet KOH etching through Si(100) wafer was conducted, using previously fabricated square-shaped windows as a mask. KOH etching of Si(100) is an anisotropic etching, which created a cavity with a trapezoidal cross-section. The etched crystallographic plane is (001) and the exposed un-etched walls of the

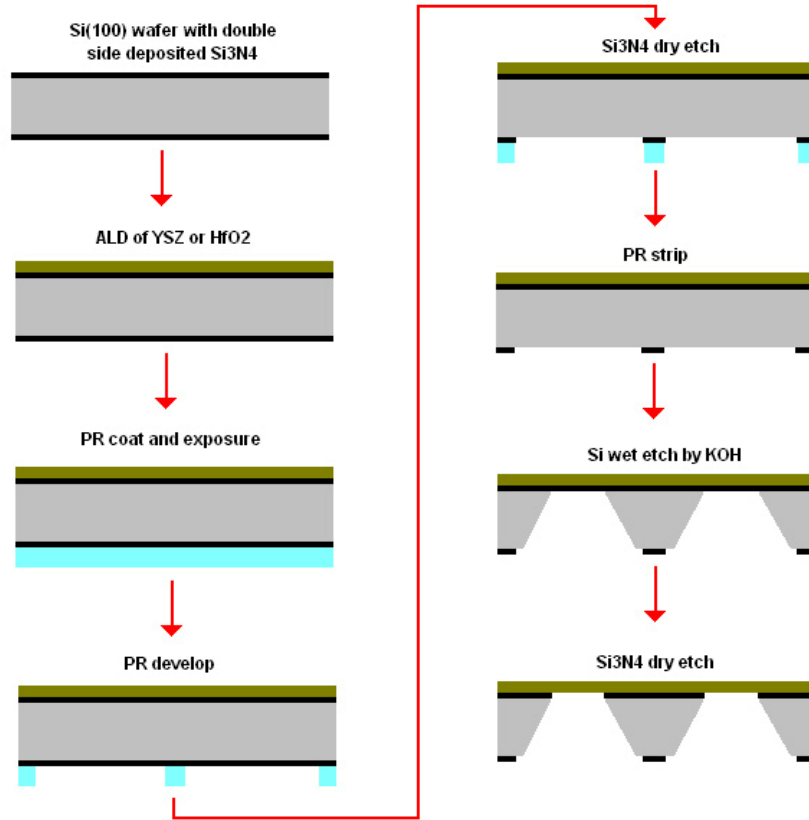


Figure 2: Flow-chart illustrating microfabrication process of ALD SOFC membrane.

cavity are (111) planes. Second Si₃N₄ layer was used as stop-layer for KOH etching of Si. The final result of KOH etching can be seen in Fig.3a. Free-standing two-layered (Si₃N₄ and HfO₂) film is homogeneous. No residues of chemical reaction were found on free-standing film and rest of the sample.

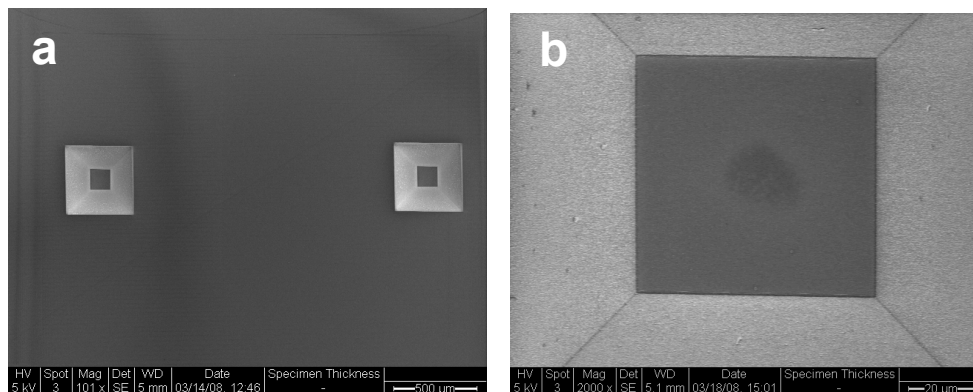


Figure 3: (a) SEM image showing KOH etched windows in Si(001). Free-standing film at the bottom of each window has layered structure: Si₃N₄ at the upper side and HfO₂ at the lower side. (b) SEM image showing HfO₂ free-standing film after dry etching of Si₃N₄ layer.

The most critical step of creating ultra-thin SOFC electrolyte membrane in form of free-standing film is removal of Si_3N_4 layer from the backside of the wafer after the KOH etching process. Free-standing HfO_2 film, having dimensions of $75 \times 75 \mu\text{m}^2$, after final RIE of Si_3N_4 for 3 min and 45 s is shown in Fig.3b. The film looks homogeneous, without residuals of chemical reaction. However, some residuals of the reaction were found on rest of the sample. After RIE, many windows appeared to be broken or cracked, probably due to large internal stress in annealed HfO_2 film. HfO_2 crystallization from the amorphous phase is followed by considerable volume change, which introduces significant stress in the films. Hence, ultra-thin free-standing films having large area compared to their thickness can be easily broken by careless handling of the sample or can be self-cracked after RIE process. Most surviving windows had a smallest size from 4 various fabricated sizes. This observation suggests that larger windows have larger numbers of defects which could initiate cracking. Auger electron spectroscopy (AES) results showed a mixed elemental composition for the free-standing film surface from the etched side after final RIE of Si_3N_4 for 3 min and 45 s. Quantitative analysis was not performed due to strong overlap of Si2 and Hf2 peaks. Strong peaks of Si, O and N were revealed; however, Hf peaks were considerably weaker (Fig.4a). For comparison, strong Hf signal was obtained from the HfO_2 (top) side of the wafer, showing HfO_2 composition of the film (Fig.4b). The possible reason for this result is existence of ultra-thin interlayer between Si_3N_4 and HfO_2 , which wasn't been removed by RIE. Existence of such layer was confirmed by TEM cross-section characterization of HfO_2 films deposited directly on Si (TEM results in section 2), and can be suggested by mixed interface composition in AES profile (Fig.4c). Interstitial O^{2-} and OH^- species incorporated in HfO_2 during film growth can cause SiO_2 growth at the interface during post-processing, as shown by experiment.⁵

Successful removal of this interlayer was done by applying longer RIE time using same recipe for nitride etch. This recipe has slower etching rate for SiO_2 , which can be possible interlayer material. AES of the free-standing HfO_2 film without interlayer material is shown in Fig.4d.

In this part of the project, we have shown the ability to create free-standing ultra-thin electrolyte membrane for individual SOFC, which later should be covered from both sides by electrodes. The next step in this part of the project is optimization of window size (or free-standing film size) and membrane thickness in order to obtain larger number of non-cracked free-standing films. Furthermore, RIE conditions in the last stage of the microfabrication process (Fig.2) have also be optimized for the same purpose.

Successful removal of this interlayer was done by applying longer RIE time using same recipe for nitride etch. This recipe has slower etching rate for SiO_2 , which can be possible interlayer material. AES of the free-standing HfO_2 film without interlayer material is shown in Fig.4d.

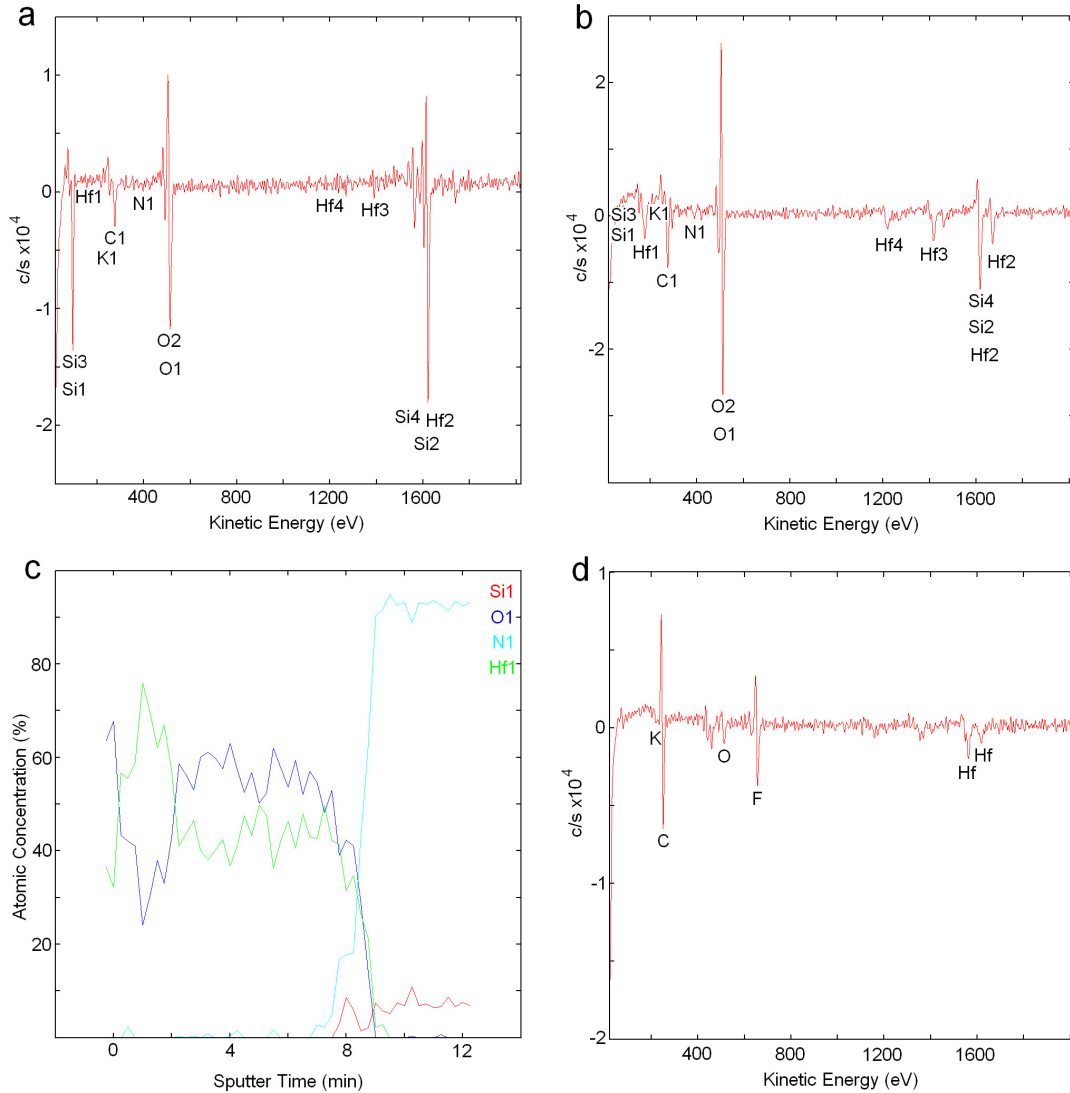


Figure 4: AES spectrum taken from the etched side (3 min 45 s dry etch) (a), and from the HfO₂ (top) side (b). (c) AES profile from the HfO₂ (top) side into Si₃N₄ layer. (d) AES spectrum taken from the etched side (4 min 15 s dry etch).

In this part of the project, we have shown the ability to create free-standing ultra-thin electrolyte membrane for individual SOFC, which later should be covered from both sides by electrodes. The next step in this part of the project is optimization of window size (or free-standing film size) and membrane thickness in order to obtain larger number of non-cracked free-standing films. Furthermore, RIE conditions in the last stage of the microfabrication process (Fig.2) have also be optimized for the same purpose.

2. Metal Oxide Nanotubes by ALD

For fabrication of well defined, vertical HfO₂ nanotubes with conformal wall thickness, pre-grown vertical Ge nanowires were used. Similar to the planar free-standing window fabrication described in section 1, above, we have focused on HfO₂ in our initial

studies of nanotube synthesis because it is easier to deposit than YSZ (no laminate rowth required) and its chemical and etching properties are similar. Ge(111) nanowires on Si(111) substrates were grown using the vapor-liquid-solid (VLS) method and these wires were used as template for HfO_2 nanotube fabrication by ALD. The initial Ge nanowires outer diameter defined the inner diameter of the final metal oxide nanotubes. HfO_2 nanotubes process sequence includes steps illustrated by flow-chart in Fig.5.

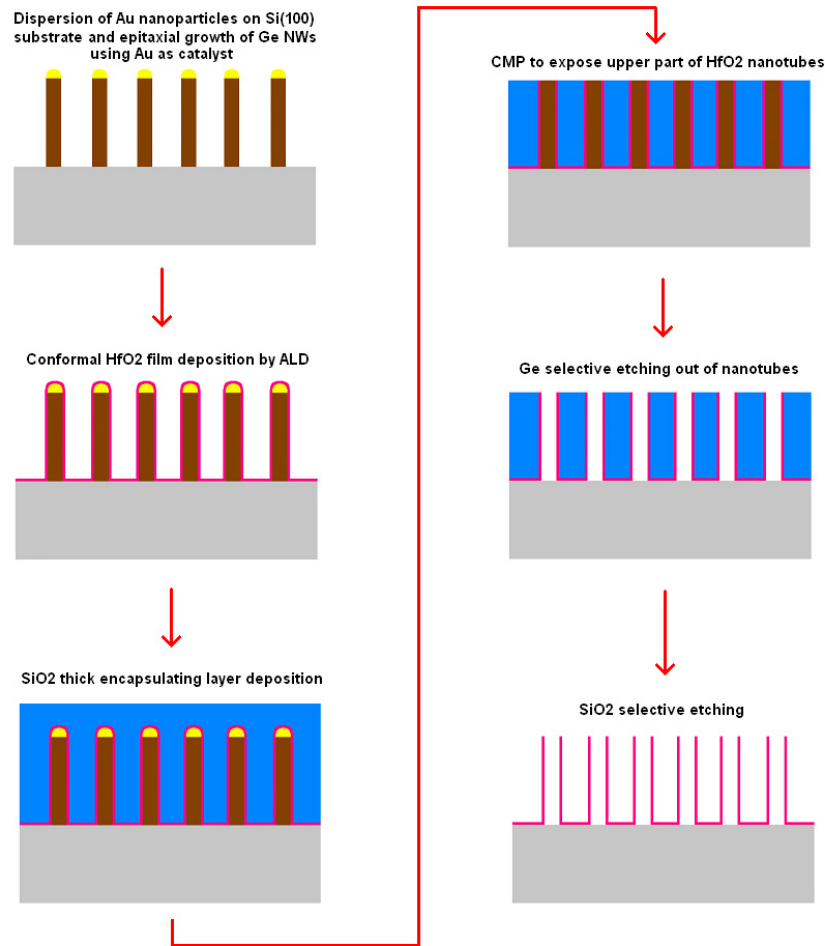


Figure 5: Flow-chart illustrating oxide nanotubes process sequence.

For the initial experiments, Ge selective wet etching was applied to broken Ge nanowires on Si substrate covered by ALD HfO_2 (see second step in Fig.5). After HfO_2 deposition, the samples were annealed at 800 and 850°C in He atmosphere for 3 hrs in order to crystallize as-deposited amorphous HfO_2 . Ge is highly susceptible to aqueous corrosion as result of solubility of GeO_2 in water. First results showed that Ge nanowires were dissolved after few minutes in 30% H_2O_2 aqueous solution at 40°C in ultrasonic bath. These conditions did not produce any etching of HfO_2 thin films. SEM characterization of the etched samples showed hollow broken HfO_2 nanotubes (Fig.5). Unbroken Ge nanowires covered by HfO_2 were not etched, since H_2O_2 solution could not reach encapsulated Ge core.

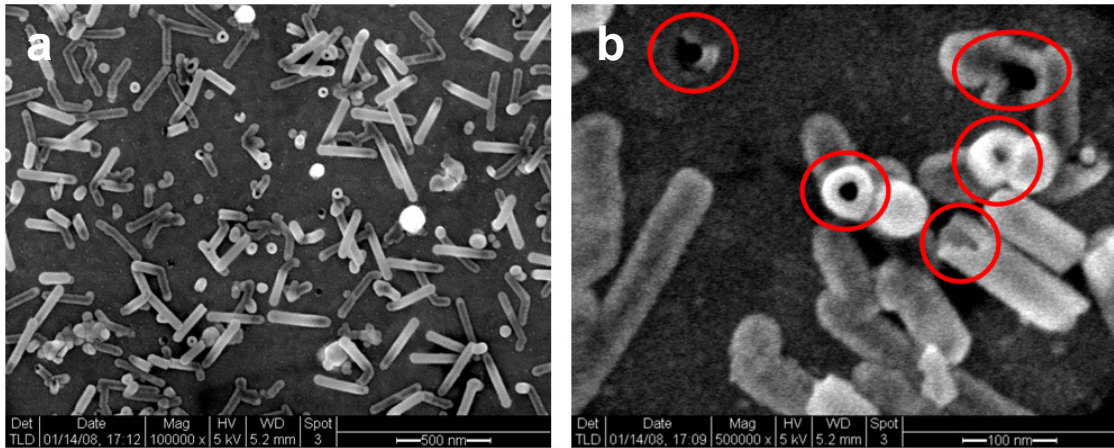


Figure 6: SEM images showing broken hollow HfO₂ nanotubes after Ge removal process: (a) low magnification, (b) high magnification.

Complete removal of Ge core in broken nanotubes was confirmed by TEM. Cross-section TEM samples were prepared by mechanical thinning of the samples glued face-to-face using diamond lapping papers and further ion milling at low angle. High-resolution TEM (HRTEM) images of cross-sectioned samples showed a hollow HfO₂ tubes without sign of remaining Ge (Fig.7a).

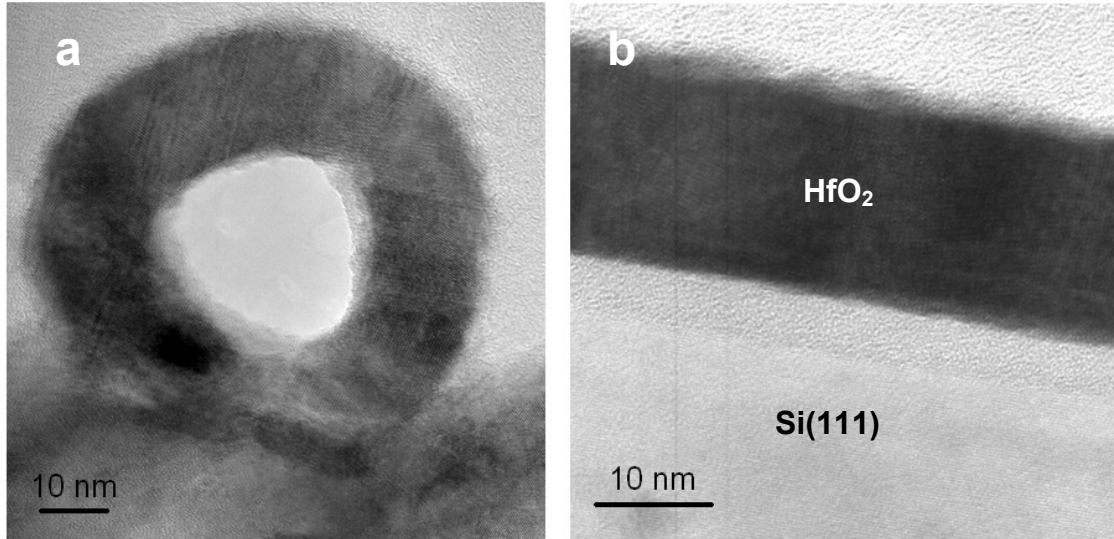


Figure 7: HRTEM cross-section images showing HfO₂ nanotube after selective Ge wet etching (a), and HfO₂ layer on Si(111) substrate.

TEM EDS analysis of broken nanotubes also confirmed absence of Ge (Fig.8). TEM characterization confirmed full crystallization of HfO₂ and high degree of film conformity on both Si substrate and Ge nanowires. Single-phase monoclinic HfO₂ was identified using selected area electron diffraction (SAED) in HfO₂ nanotubes and HfO₂ film on Si substrate (Figs. 9a and 9b). No preferred crystallographic orientation of HfO₂

nanocrystals within films was observed in HRTEM images and SAED. ALD HfO₂ films had thickness ranged from 15 to 26 nm. We plan to decrease film thickness below 5 nm in order to obtain other possible phases of HfO₂ ultra-thin films, such as tetragonal, orthorhombic and cubic phases.

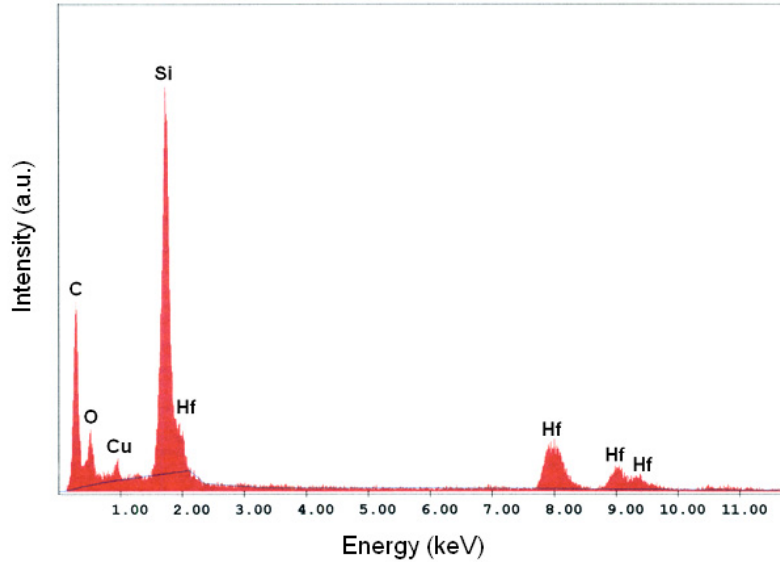


Figure 8: EDS analysis showing absence of residual Ge after selective wet etching. Note that Cu contamination is from TEM grid after ion milling of the sample.

The phase stabilization can be obtained by reduction of the crystal size. The monoclinic to tetragonal phase transition occurs in bulk at 1720°C. In thin films, the monoclinic phase transforms to the tetragonal or orthorhombic and eventually to the cubic (transitions at much lower temperatures 500–900°C).⁶

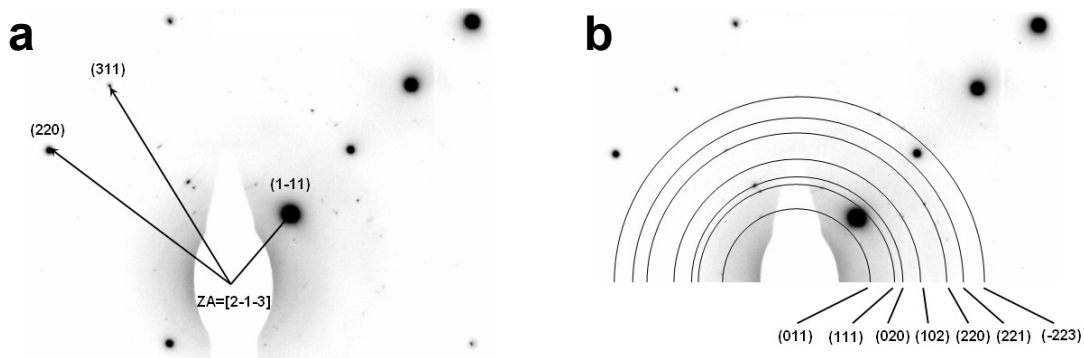


Figure 9: SAED from HfO₂ nanotubes and Si(111) substrate showing Si spot pattern and HfO₂ ring pattern (rings were drawn due to small amount HfO₂ nanocrystals that produced small amount of diffraction spots inside each ring).

An ultra-thin (~5 nm) amorphous interfacial layer was observed between Si and HfO₂ (Fig.7b). As mentioned in section 1, interstitial O²⁻ and OH⁻ species incorporated in HfO₂ during film growth can cause SiO₂ growth at the interface during post-deposition annealing.

Following flow-chart in Fig.5, Ge nanowires were further encapsulated by thick SiO₂ layer (Fig.10) as preparation step for CMP process. SiO₂ layer was deposited using plasma enhanced chemical vapor deposition (PECVD).

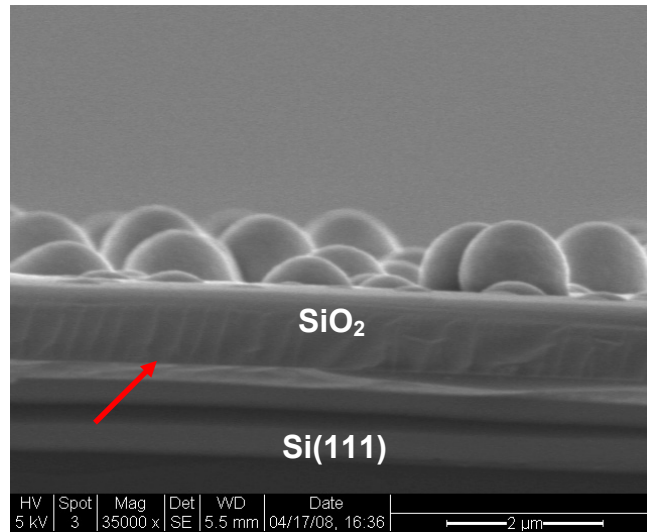


Figure 10: SEM X-section image showing nanowires encapsulated by thick SiO₂ layer. Interface between Si substrate and SiO₂ layer is marked by arrow.

In this part of the project, we have shown ability to selectively etch Ge core from HfO₂ nanotubes, and have conducted detailed structural characterization of HfO₂ nanotubes and films. The next step in this part of the research is to apply CMP in order to expose upper parts of HfO₂ nanotubes (fourth step in Fig.5) and etch out Ge and SiO₂ materials. We will also extend the research to ALD-YSZ nanotubes. Then, crystal structures of nanotubes with various wall thicknesses will be studied.

3. ALD Process Development for LSCO Electrodes

Achieving ALD growth is simple in theory, but often difficult in practice. This is particularly true for deposition of multicomponent alloys (e.g. YSZ) or of complex compounds (e.g. LaSrCoO_x – LSCO), which are of interest in the present project. Factors that influence film growth include:

1. Precursor chemistry
2. Oxidant choice
3. Precursor delivery flow rate
4. Oxidant delivery flow rate
5. Precursor source temperature and vapor pressure
6. Main chamber pressure
7. Precursor and oxidant dosage
8. Chamber purge times

Much of the progress so far has been in the development of suitable deposition parameters for individual oxides. Achieving ALD of individual oxides first gives us an

approximate starting point for nanolaminate deposition parameters, though growth characteristics are likely to change once these films are grown on top of each other.

Precursor Chemistry

The choice of precursor influences the source temperature (via vapor pressure), substrate temperature, and oxidant. Initial individual oxide depositions involved the use of tetramethyl-3,5-heptanedioate-based, or (tmhd)-based, precursors. These chemicals, also known as β -diketonates, have low volatility and low reactivity, and were most effectively paired with oxygen plasma as an oxidant. Furthermore, the low volatility required the use of higher temperature lines, and thus special high-temperature materials. However, we initially chose (thmd)-based precursors as they were readily available for all three components, and their chemical compatibility made them attractive.

In practice, supplying enough precursor gas to the main chamber proved problematic and the use of oxygen plasma introduced processing obstacles that soon made other precursor chemistries more attractive. After searching for higher volatility precursors that react readily with water, we currently have switched to cyclopentadienyl-based precursors for the strontium and lanthanum oxides, and a new amidinate-based precursor for cobalt oxide. Individual oxide results will be discussed in the following sections.

Lanthanum Oxide

Uniform lanthanum oxide films were achieved using lanthanum tris(isopropyl-cyclopentadienyl) supplied by Strem Chemicals and water as oxidant. In our ALD setup, due to the large chamber and long delivery line lengths, achievement of uniform films is particularly sensitive to source and line temperatures, gas flow, dosage, and purge times. Figure 11 shows a thickness map of an lanthanum oxide film deposited via ALD in our chamber, as measured by ellipsometry ($n = 1.76$).

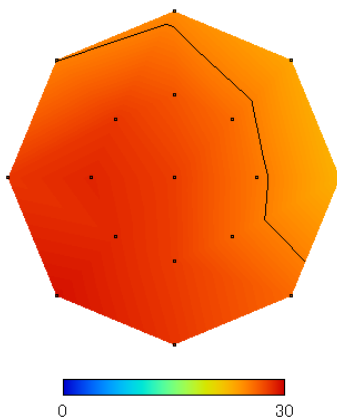


Figure 11: Thickness map of lanthanum oxide deposited, as measured by ellipsometry. The minimum measured thickness was 22.6 Å and the maximum measured thickness was 29.3 Å. Average thickness was 26.5 Å with a standard deviation of 1.9 Å.

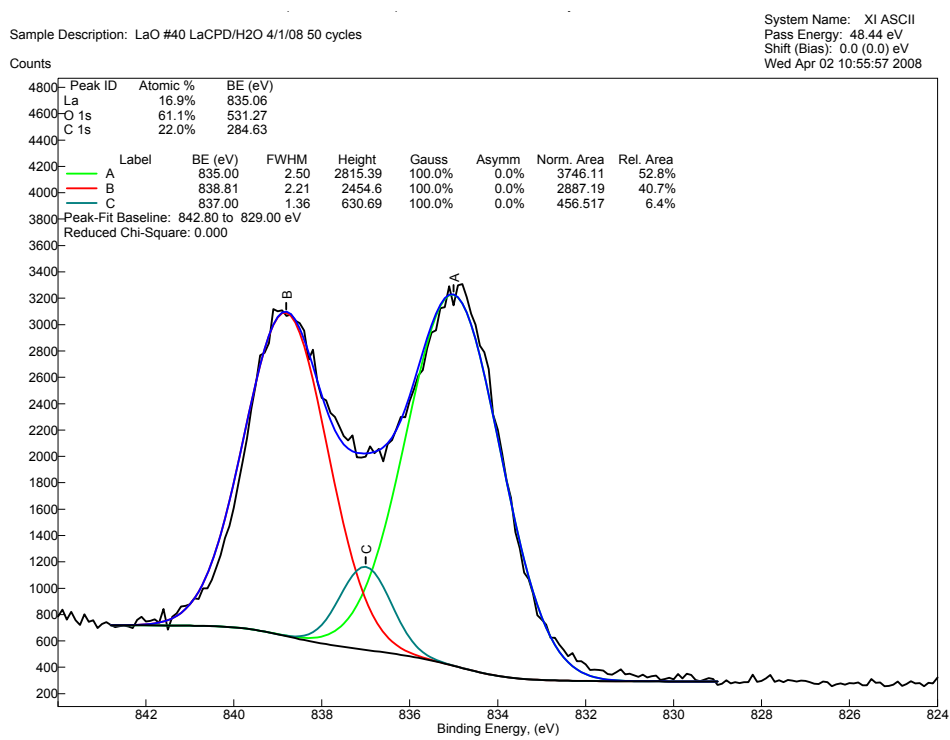
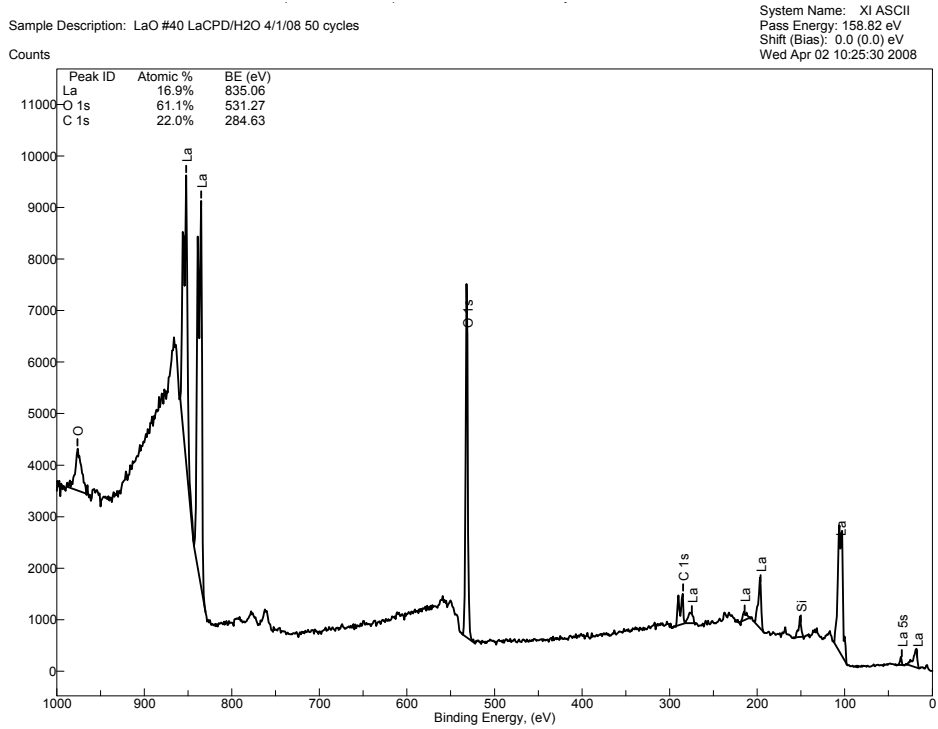


Figure 12: XPS survey and high-resolution scan results for roughly 30 Å of La₂O₃ grown via ALD. The survey scan shows no contaminants or chemical decomposition of the precursor, and the high resolution scan shows a peak at binding energy 835.0 eV, which corresponds to the La-3d^{5/2} peak in La₂O₃.⁷

X-ray photoelectron spectroscopy (XPS) results (Figure 12) confirm the growth of La_2O_3 films. The ALD optimization of lanthanum oxide is mostly complete.

Strontium Oxide

Attempts to use a β -diketonate precursor to deposit strontium oxide were largely unsuccessful. Strontium bis(2,2,6,6-tetramethyl-3,5-heptanedionate), or $\text{Sr}(\text{tmhd})_2$, required a high source temperature of over 200°C to obtain a nominal vapor pressure, making it difficult to work with due to the need for high-temperature equipment and sufficient insulation. Furthermore, the precursor was largely unreactive with anything besides oxygen plasma, making it difficult to work within our chamber.

Recent depositions have shown some progress in attaining reasonable ALD of strontium oxide. We switched to a cyclopentadienyl-based precursor, strontium bis(isopropylcyclopentadienyl), which offers much more volatility at lower source temperatures (around $120\text{-}140^\circ\text{C}$), while being reactive enough to use water as an oxidant. Figure 13 shows a thickness map of a strontium oxide film grown via ALD, using ellipsometry and a refractive index of 1.89 .⁸

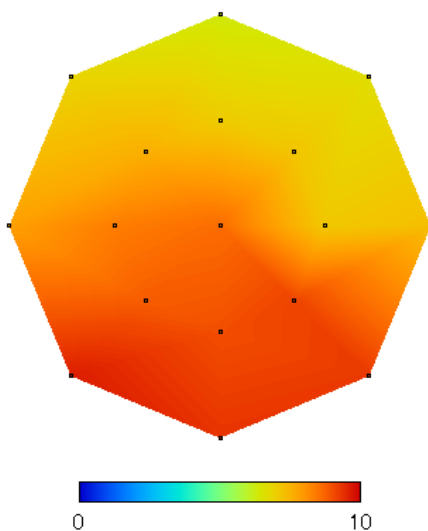


Figure 13: Thickness map of strontium oxide deposited on a silicon wafer, as measured by ellipsometry. The minimum measured thickness was 6.3 \AA and the maximum measured thickness was 9.6 \AA . Average thickness was 8.0 \AA with a standard deviation of 1.1 \AA . This corresponds to a growth per cycle of approximately 0.16 \AA/cycle , comparable to values of approximately 0.2 \AA/cycle as reported by Holme, *et. al.*⁹

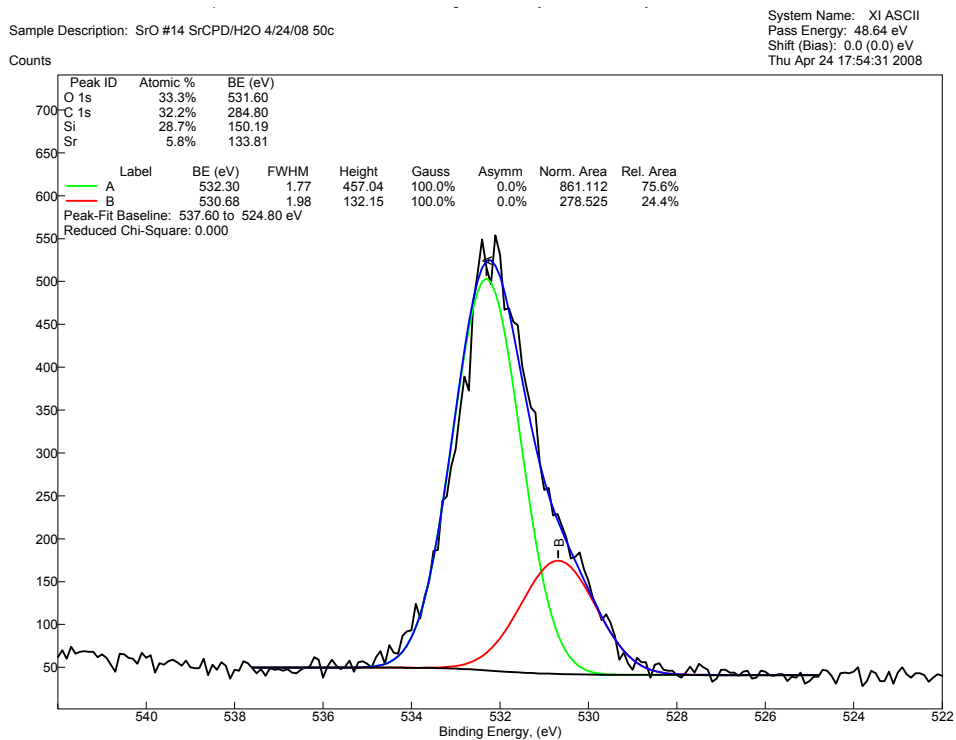
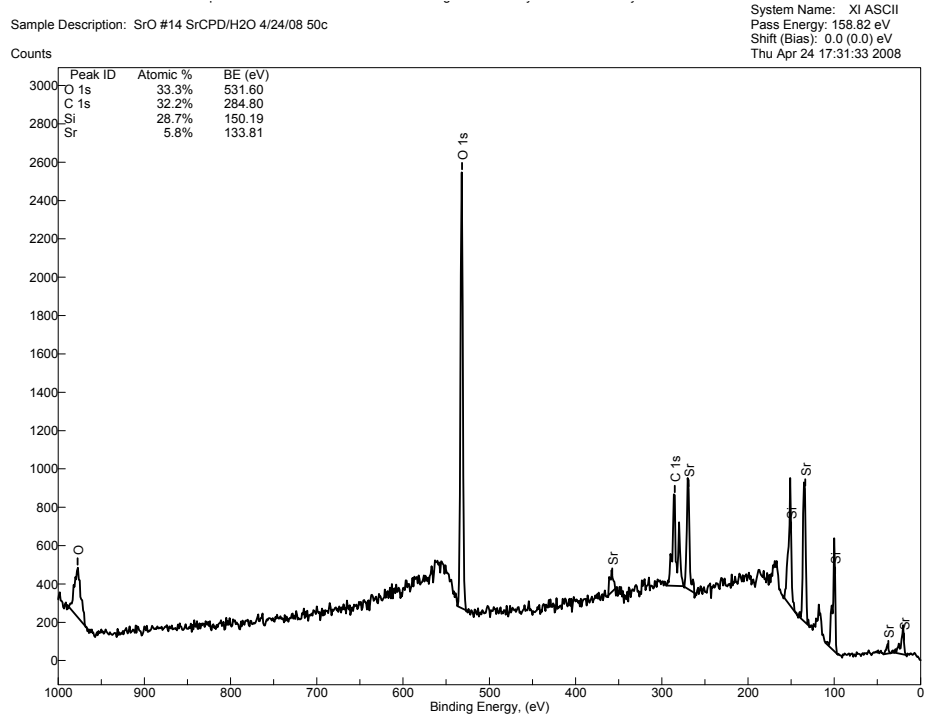


Figure 14: XPS survey and high-resolution scan results for roughly 10Å of SrO grown via ALD. The survey scan shows no contaminants or chemical decomposition of the precursor, and the high resolution scan shows a chemically shifted oxygen peak at adjusted binding energy 530.0 eV, which corresponds to the presence of SrO.¹⁰

X-ray photoelectron spectroscopy (XPS) results confirm the growth of SrO films (Figure 14). Further experiments to achieve better uniformity will be made in the future.

Cobalt Oxide

Cobalt oxide deposition using a (tmhd)-based precursor was the most successful of the three individual oxides deposited using β -diketonates, but still relied on the use of oxygen plasma as oxidant. To eliminate problems associated with using plasma in our chamber as well as enhance compatibility with the other precursors using water as an oxidant, we replaced the (tmhd)-based precursor with a new amidinate-based precursor just introduced by Rohm & Haas at a recent ALD conference.

This new precursor is extremely volatile. Initial deposition attempts used much too high a source temperature (78°C), but we were able to confirm the growth of cobalt oxide. Initial depositions exhibited CVD-like conditions due to the high source temperature, but later depositions showed ALD-like uniformity.

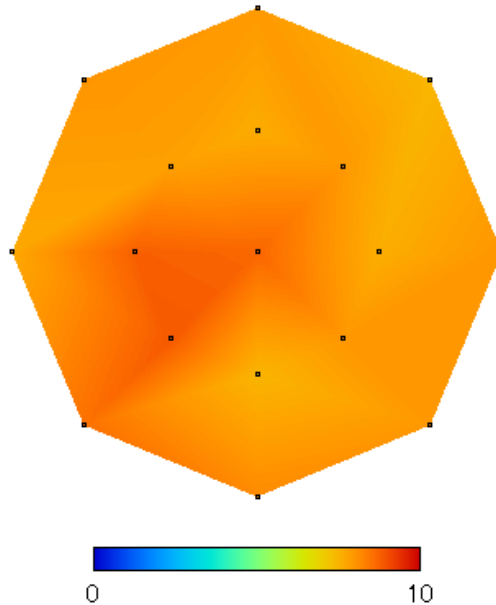


Figure 15: Thickness map of cobalt oxide deposited on a silicon wafer, as measured by ellipsometry. The minimum measured thickness was 7.5 Å and the maximum measured thickness was 8.9 Å. Average thickness was 8.0 Å with a standard deviation of 0.4 Å.

This corresponds to a growth per cycle of 0.16 Å/cycle, comparable to values of approximately 0.2 Å/cycle as reported by Klepper, *et al.*¹¹

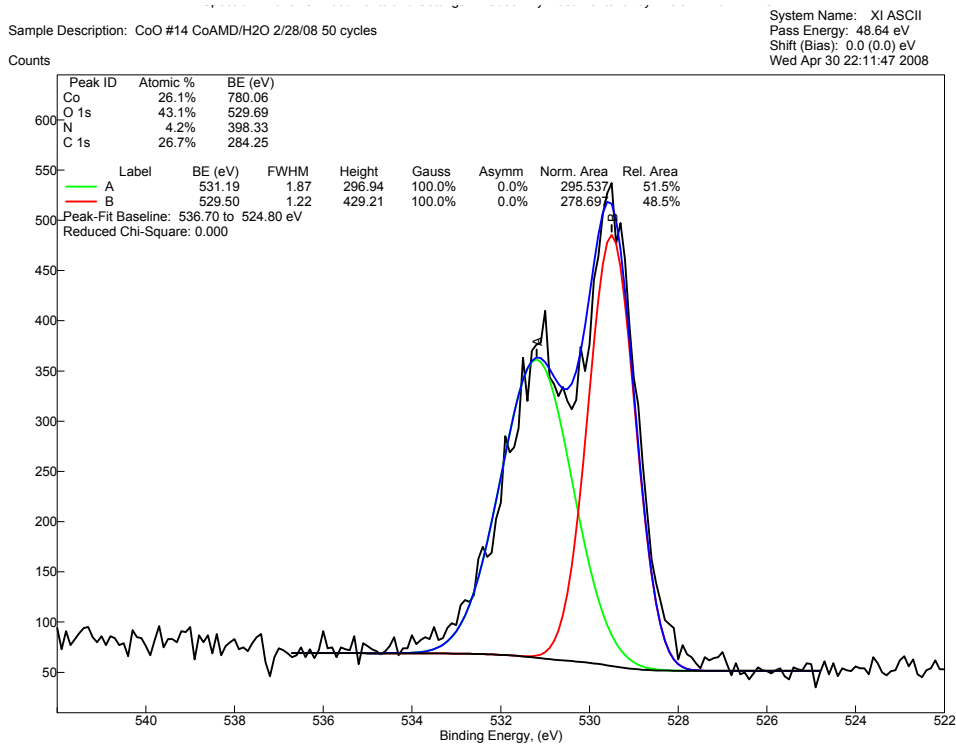
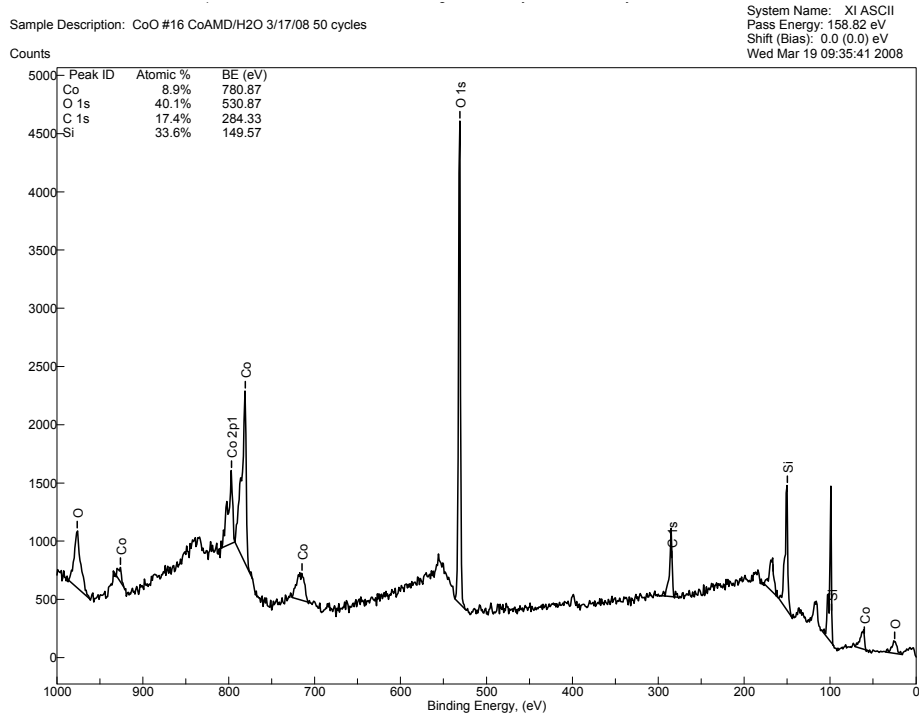


Figure 16: XPS survey and high-resolution scan results for CoO grown via ALD. The survey scan shows no contaminants or chemical decomposition of the precursor and the high resolution scan shows chemically shifted oxygen peaks at binding energies 529.5 and 531.2 eV, which corresponds to the presence of CoO.⁴

Lanthanum Strontium Cobalt Oxide

A nanolaminate of lanthanum strontium cobalt oxide has not yet been attempted. However, a reasonable optimization of the individual oxides has been achieved, so nanolaminate deposition experiments are planned for the coming weeks. After optimization of the nanolaminate composition is performed, we will conduct annealing experiments to test for formation of the desired perovskite crystal structure and will measure oxygen diffusion through the film. The electronic and ionic conductivities of the LSCO layer will be measured by temperature-dependent I-V characterization and impedance spectroscopy, in collaboration with Prof. Ramanathan's group at Harvard.

4. Variable Temperature Micro-SOFC Test System

The goal of our investigation is to optimize the fabrication of free-standing SOFC thin films. As described earlier, electrodes and electrolyte sequentially deposited onto a silicon wafer using the atomic layer deposition (ALD) technique. In order to ascertain the effectiveness of the fabrication process being investigated, it is critical to have an apparatus capable of rapidly characterizing the electrical properties of the fabricated device. In so doing, the turnaround time on each design iteration will be greatly reduced.

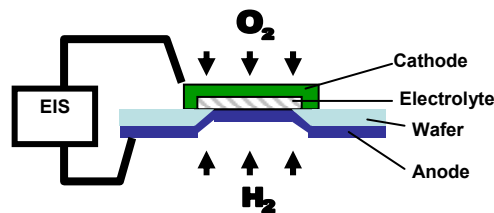


Figure 17: Schematic layout of micro-SOFC test geometry (free-standing electrolyte).

In the fuel cell, the anode will be exposed to hydrogen while the cathode will be exposed to the air. Moreover, for the device to operate efficiently, the film and gas must be heated; this enhances the rate of oxygen ion conduction and the electrode exchange kinetics. To create conditions necessary for the efficient operation of these fuel cells, a test setup was designed and will be constructed in the coming weeks (Fig. 18).

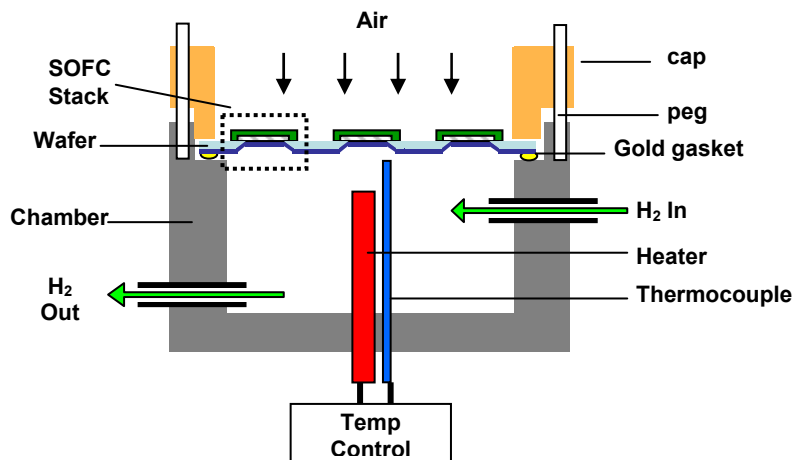


Figure 18: Design of SOFC test setup.

The test apparatus will consist of a cylindrical Inconel chamber open at the top. The wafer will be placed on the top of the chamber and held down firmly using a weighted cap to provide pressure for seal. Next, hydrogen with a known pressure and concentration can be flowed into the chamber. Heat will be provided by a halogen lamp and regulated using a thermocouple with a PID temperature controller.

Having created the appropriate conditions, individual fuel cell windows can be probed and measured. For this purpose, the ac impedance spectroscopy technique will be employed to investigate the electrical properties of the fuel cell stacks. This procedure is widely used because it allows us to readily identify the individual contributions of heterogeneous interfaces, grain boundaries, surfaces, and space charges to the overall fuel cell performance.¹² Such information is invaluable, as it could help us to pinpoint problematic fabrication stages.

With this apparatus, which is now designed and will soon be fabricated, we should be capable of rapidly testing the I-V characteristics of fabricated SOFC devices in our laboratory. Ultimately, we expect this will greatly enhance the speed with which we can optimize the fabrication process. This work will be synergistic with the more sophisticated electrochemical testing to be undertaken by our collaborators at Harvard.

Progress

The potential impact of the research on global warming gas emissions during automotive transportation is substantial, if the various process steps demonstrated and/or optimized individually this year (see **Results** section) can be successfully integrated to make highly efficient, high-power-density SOFCs in an economical fashion. In particular, the first demonstration of ALD-derived metal oxide nanotubes, which is described in that section of the report, holds the promise for greatly enhancing the effective surface area of SOFC membranes and lowering operating temperatures by thinning the electrolyte layer substantially. Development of an ALD process for $\text{La}_2\text{O}_3/\text{SrO}/\text{CoO}$ nanolaminates, needed to synthesize conformal mixed ionic/electronic conducting electrode layers for these high aspect ratio structures, appears to be close-at-hand. This year's progress toward the goals of the project has, therefore, been satisfactory. The basic idea we are pursuing still appears to be viable and potentially game-changing, given the high efficiencies and fuel flexibility possible with SOFCs.

Future Plans

In the coming year, we plan a systematic investigation of the in-plane and through-thickness I-V characteristics of YSZ-laminate derived electrolytes of various compositions and thicknesses. We will also study pure ZrO_2 (tetragonal) and HfO_2 (monoclinic phase) to understand how crystal structure in the fluorite metal oxides affects oxygen ion transport in nanocrystalline films. Through-thickness measurements will use the free-standing ALD-grown metal oxides demonstrated in the past year of the project, with either very thin (porous) Pt electrodes or ALD-grown LSCO electrodes. We will also work on preparation of high surface area ALD electrolytes using the Ge nanotube templating approach demonstrated in this year's research. Variable temperature through-thickness I-V measurements will be performed using the recently-designed, controlled

atmosphere-heating system which we plan to construct in the next few months. In-plane measurements and more sophisticated electrochemical studies will be performed in collaboration with Prof. Ramanathan's group at Harvard. We will also supply ALD films to his group for their UV illumination experiments.

Publications

1. Ginestra, C.N., Sreenivasan, R., Karthikeyan, A., Ramanathan, S. and McIntyre, P.C. Atomic Layer Deposition of Y_2O_3/ZrO_2 Nanolaminates: A Route to Ultrathin Solid-State Electrolyte Membranes, *Electrochem. Solid-State Lett.* **10**, B161-65 (2007).
2. Ginestra, C.N., Sreenivasan, R., Karthikeyan, A., Ramanathan, S. and McIntyre, P.C. McIntyre, Atomic Layer Deposition of Y_2O_3/ZrO_2 Nanolaminates for Ultra-Thin Solid State Electrolyte Alloys, 7th International Conference on Atomic Layer Deposition, San Diego, CA June 24-27. (oral presentation).

References

1. Ginestra, C.N., Sreenivasan, R., Karthikeyan, A., Ramanathan, S. and McIntyre, P.C. Atomic Layer Deposition of Y_2O_3/ZrO_2 Nanolaminates: A Route to Ultrathin Solid-State Electrolyte Membranes. *Electrochem. Solid-State Lett.* **10**, B161-65 (2007).
2. Brahim, C., Ringuede, A., Cassir, M., Putkonen, M. and Niinisto, L. Electrical Properties of Thin Yttria-Stabilized Zirconia Overlayers Produced by Atomic Layer Deposition for Solid Oxide Fuel Cell Applications. *Appl. Surf. Sci.* **25**, 3962-68 (2007).
3. Shim, J.H., Chao, C-C., Huang, H., and Prinz, F.B. Atomic Layer Deposition of Yttria-Stabilized Zirconia for Solid Oxide Fuel Cells. *Chem. Mater.* **19**, 3850-54 (2007).
4. Ginestra, C.N., Sreenivasan, R., Karthikeyan, A., Ramanathan, S. and McIntyre, P.C. McIntyre. Atomic Layer Deposition of Y_2O_3/ZrO_2 Nanolaminates for Ultra-Thin Solid State Electrolyte Alloys. 7th International Conference on Atomic Layer Deposition, San Diego, CA June 24-27. (oral presentation).
5. Ho, M-T., Wang, Y., Brewer, R.T., Wielunski, L.S., Moumen, N., Chabal Y.J. and Boleslawski, M. In situ Infrared Spectroscopy of Hafnium Oxide Growth on Hydrogen-Terminated Silicon Surfaces by Atomic Layer Deposition. *Appl. Phys. Lett.*, **87**, 133103/1-133103/3 (2005).
6. Ferrieu, F., Dabertrand, K., Lhostis, S., Ivanova, V., Martinez, E., Licitra C. and Rolland, G. Observation of HfO_2 Thin Films by Deep UV Spectroscopic Ellipsometry. *J. Non-Cryst. Solids*, **353**, 658-662 (2007).
7. Jo, S., *et al.* 5 nm thick lanthanum oxide thin films grown on Si(100) by atomic layer deposition: the effect of post-annealing on the electrical properties. *Thin Solid Films.* **513**, 253-257 (2006).
8. Pynchon, G. & Sieckmann, E. Refractive index of strontium oxide. *Physical Review.* **143**, 2, 595-596 (1965).
9. Holme, T., *et al.* Atomic layer deposition of LSM cathodes for solid oxide fuel cells. *Solid State Ion.* (2008).
10. Dupin, J., *et al.* Systematic XPS studies of metal oxides, hydroxides and peroxides. *Phys. Chem. Chem. Phys.* **2**, 1319-1324 (2000).
11. Klepper, K.B. *et al.* Growth of thin films of Co_3O_4 by atomic layer deposition. *Thin Solid Films.* **515**, 7772-7781 (2007).
12. Tsuchiya, M., Bojarczuk, N.A. and Ramanathan, S. Molecular beam synthesis and high temperature electrical properties of crystalline ceria thin films. *Appl Phys Lett.* **91**, 223101 (2007).

Contacts

Paul C. McIntyre: pcml@stanford.edu
Michael Shandalov: michash@stanford.edu
Nana Ayensu: nmayensu@stanford.edu
Cynthia Ginestra: ginestra@stanford.edu,
Irene Goldthorpe: goldthorpe@stanford.edu
Andy Lin: aylin@stanford.edu